ORIGINAL RESEARCH

American Heart Association | American Stroke Association

Loss of Function in Heparan Sulfate Elongation Genes *EXT1* and *EXT 2* Results in Improved Nitric Oxide Bioavailability and Endothelial Function

H. L. Mooij, MD; P. Cabrales, PhD; S. J. Bernelot Moens, MD; D. Xu, PhD; S. D. Udayappan, MSc; A. G. Tsai, PhD; M. A. J. van der Sande, MD; E. de Groot, MD, PhD; M. Intaglietta, PhD; J. J. P. Kastelein, MD, PhD; G. M. Dallinga-Thie, PhD; J. D. Esko, PhD; E. S. Stroes, MD, PhD; M. Nieuwdorp, MD, PhD

***Background*—**Heparanase is the major enzyme involved in degradation of endothelial heparan sulfates, which is associated with impaired endothelial nitric oxide synthesis. However, the effect of heparan sulfate chain length in relation to endothelial function and nitric oxide availability has never been investigated. We studied the effect of heterozygous mutations in heparan sulfate elongation genes *EXT1* and *EXT2* on endothelial function in vitro as well as in vivo.

***Methods and Result*—**Flow-mediated dilation, a marker of nitric oxide bioavailability, was studied in $Ext1^{+/-}$ and $Ext2^{+/-}$ mice versus controls (n=7 per group), as well as in human subjects with heterozygous loss of function mutations in *EXT1* and *EXT2* (n=13 hereditary multiple exostoses and n=13 controls). Endothelial function was measured in microvascular endothelial cells under laminar flow with or without siRNA targeting *EXT1* or *EXT2*. Endothelial glycocalyx and maximal arteriolar dilatation were significantly altered in $Ext1^{+/-}$ and $Ext2^{+/-}$ mice compared to wild-type littermates (glycocalyx: wild-type 0.67±0.1 μm, $Ext1^{+/-}$ 0.28±0.1 μm and $Ext2^{+/-}$ 0.25±0.1 μm, $P<0.01$, maximal arteriolar dilation during reperfusion: wild-type 11.3±1.0%), $Ext1^{+/-}$ 15.2±1.4% and $Ext2^{+/-}$ 13.8±1.6% $P<0.05$). In humans, brachial artery flow-mediated dilation was significantly increased in hereditary multiple exostoses patients (hereditary multiple exostoses 8.1±0.8% versus control 5.6±0.7%, $P<0.05$). In line, silencing of microvascular endothelial cell *EXT1* and *EXT2* under flow led to significant upregulation of endothelial nitric oxide synthesis and phospho-endothelial nitric oxide synthesis protein expression.

***Conclusions*—**Our data implicate that heparan sulfate elongation genes *EXT1* and *EXT2* are involved in maintaining endothelial homeostasis, presumably via increased nitric oxide bioavailability. **(*J Am Heart Assoc*.2014;3:e001274 doi: 10.1161/JAHA.114.001274)**

Key Words: endothelial function • EXT • heparan sulfate • nitric oxide

Despite all therapeutic progress achieved in the last decades, cardiovascular disease is still one of the leading causes of mortality in Western countries.[1] Endothelial dysfunction, an indicator of decreased endothelial nitric oxide (NO) bioavailability, has been acknowledged as the earliest stage of vascular damage, preceding the manifestation of cardiovascular disease.[2,3] The central factor determining basal NO activity is thought to be shear-induced endothelial activation via mechanosensing of the endothelial glycocalyx,[4] which consists of a mesh of proteoglycans and glycosaminoglycans including heparan sulfate proteoglycan (HSPG) and hyaluronan, covering the luminal endothelial wall. Damage to the endothelial glycocalyx has been associated with attenuated shear-mediated NO release by the endothelium as shown in both in vitro and in vivo studies.[5–9] In line, chronic exposure to increased plasma glycocalyx degrading enzymes including hyaluronidase and heparanase has been shown to lead to accelerated atherosclerotic plaque formation in mice[10,11] as well as reduced NO production in vitro.[12,13] Yet, the precise role of the individual components of the endothelial glycocalyx in mediating mechanotransduction remains to be established.

HSPGs contain heparan sulfate chains on a proteoglycan (PG) backbone. The assembly of the chains is catalyzed by members of the exostosin family (EXT) involved in initiation

From the Department of Vascular Medicine, AMC-UvA, Amsterdam, The Netherlands (H.L.M., S.J.B.M., S.D.U., E.G., J.J.P.K., G.M.D.-T., E.S.S., M.N.); Departments of Bioengineering (P.C., A.G.T., M.I.) and Cellular and Molecular Medicine (D.X., J.D.E.), UC San Diego, CA; Department of Orthopedics, Leiden University Medical Center, Leiden, The Netherlands (M.A.J.S.).

Correspondence to: M. Nieuwdorp, MD, PhD, Department of Vascular Medicine, Academic Medical Center Amsterdam, Meibergdreef 9, room F4-159.2, 1105 AZ Amsterdam, the Netherlands. E-mail: m.nieuwdorp@amc.uva.nl

Received July 31, 2014; accepted October 19, 2014.

and chain elongation, and *N*-deacetylase/*N*-sulfotransferase and *O*-sulfotransferase involved in chain sulfation.[14,15] HSPGs play a regulating role in many biological processes including fine-tuning developmental and physiological processes, and their alteration can underlie pathological changes in lipid metabolism and inflammation.[16]

In humans, heterozygous loss of function mutation in *EXT1* and *EXT2* are known to be involved in the development of HME syndrome,[17] a disorder associated with bony tumor formation,[18,19] with a reported prevalence of 1/50 000 individuals.[20] In these subjects, these loss-of-function mutations have been shown to lead to alterations in the structure of tissue and plasma heparan sulfate composition.[21,22]

Despite the ubiquitous expression of *EXT* genes throughout the human body,[16] endothelial derangements have never been studied in humans with loss of function in *EXT* genes. In the present study, we thus investigated the effect of disrupted HSPGs on endothelial function and subsequent NO production both in vivo and in vitro.

Methods

Animal Preparation

All animals were housed in barrier conditions in the vivaria of the School of Medicine of the University of California San Diego that were approved by the Association for Assessment and Accreditation of Laboratory Animal Care; standards and procedures approved by the local Institutional Animal Care and Use Committee were followed. Mice were weaned at 3 weeks, were maintained on a 12-hour light–dark cycle, and were fed water and standard rodent chow ad libitum. All animals were fully backcrossed on a C57Bl/6 background and the presence of heterozygous state for *Ext1* or *Ext2* was established as described.[18] All investigations were performed in overnight fasted male mice (aged 12 to 16 weeks).

Male $Ext1^{+/-}$ and $Ext2^{+/-}$ as well as wild-type (WT) male littermates (n=7 per group) were fitted with a dorsal window chamber as previously described.[23] This model has been extensively used for investigations of the intact microvasculature of adipose and subcutaneous tissue and skeletal muscle in awake animals for extended periods. Animals were anesthetized with intraperitoneal ketamine and xylazine (2 mg/kg) for window implantation. After hair removal, sutures were used to lift the dorsal skin away from the animal, and 1 frame of the chamber was positioned on the animal's back. A chamber consisted of 2 identical titanium frames with a 12-mm circular window. One side of the skin fold was removed with the aid of backlighting and a stereomicroscope following the outline of the window, until only a thin layer of retractor muscle and the intact subcutaneous skin of the opposing side remained. Saline and then a cover glass were placed on the exposed skin that was held in place by the other frame of the chamber. The intact skin of the other side was exposed to the ambient environment. Following window implantation, a jugular catheter was implanted. Four days after surgery the microvasculature was examined, and only animals passing established systemic and microcirculatory inclusion criteria, which include having tissue void of low perfusion, inflammation, and edema, were entered into the study.

Experimental Setup

Unanesthetized animals were placed in a restraining tube with a longitudinal slit from which the window chamber protruded. The animals were given 60 minutes to adjust to the tube environment before measurements started. The conscious animal in the tube was then fixed to the microscopic stage of an intravital microscope (BX51WI; Olympus, New Hyde Park, NY). Detection of red blood cell passage was enhanced by increasing contrast between red blood cells and tissue using a BG12 (420 nm) bandpass filter. Arterioles, capillaries, and postcapillary venules (n=7 mice per group) were randomly selected for observation. Fluorescence images of vessels were displayed on a computer screen and recorded for subsequent analyses. The vascular images were captured with a charge-coupled device camera (ORCA-285; Hamamatsu, Japan) with 1344 × 1025-pixel resolution. Tissue fields of 175 × 140 μm were visualized with a ×40 objective (LUMPFL-WIR, NA 0.8; Olympus) and 117 × 94 μm with a ×60 objective (LUMPFL-WIR, NA 1.2; Olympus). Tissue was illuminated with a mercury burner and appropriate fluorescent cube filters were used (XF100–2 and XF02–2; Omega Optical, Brattleboro, VT) to capture fluorescence of fluorescein isothiocyanate–labeled dextran 70 kDa and Texas Red labeled dextran 40 kDa (Invitrogen). Epi-illumination of each vessel was limited to <10 s to prevent photobleaching and light-dye injury to microvessels. Brightfield and fluorescence images were analyzed using commercially available software (Image pro plus). Dye penetration analysis was completed using the inflection points of the fluorescent intensity profiles across the vessel or capillary at 3 locations, and the average value was determined. Endothelial glycocalyx thickness was calculated by subtracting the width values obtained with fluorescein isothiocyanate dextran (70 kDa) from those obtained using Texas red Dextran (40 kDa) column widths and dividing by 2, as previously published.[24]

Arteriolar Occlusions

Detailed mappings of the vasculature were made so that the same vessels were studied throughout the experiment. Arterioles (45- to 60-μm diameter and 0.5- to 1-mm length and devoid of branching) were chosen, according to their

visual clarity. The arterioles were occluded with a glass micropipette made with 1-mm-diameter glass tubing whose tip was drawn into a long fiber by a pipette puller (P-87 horizontal puller; Sutter Instruments, Novato, CA). The fiber was bent over a flame, and the knee of the bend was pressed on the intact skin of the preparation mounted on an inverted microscope, which allowed observation of the opposite side of the window chamber (ie, the intact microcirculation) (23; also see Figure 1). Arterioles were occluded for only 5 s, until flow completely stopped, and occlusion was released to prevent tissue hypoxia. Due to technical difficulties, only 4 to 6 experiments per mouse group could be analyzed. Additionally, the diameter was measured 200 μm from the occlusion point with recording of the occluded vessel starting 10 s prior to the occlusion, during the occlusion, and during 90 s after the reperfusion. The video image shearing technique was used to measure vessel diameter offline from video recordings.[25]

Endothelial Function in HME Subjects and Controls

We enrolled Dutch HME subjects (n=13), with established heterozygous loss-of-function mutations in either *EXT1* or *EXT2* (Table 1), and unrelated controls (n=13), matched for age and gender[26] since both *EXT*1 and *EXT*2 affects heparan sulfate biosynthesis. Subjects were excluded from participation if they were smoking, had a history of active malignancy with limited lifespan, cardiovascular disease, diabetes mellitus, or use of concomitant medication. Written informed consent was obtained after explanation of the study. The study was approved by the institutional review board of the Academic Medical Center of the University of Amsterdam and was carried out according to the Declaration of Helsinki.

Table 1. Mutations in *EXT1* and *EXT2*

Exon	Nucleotide Change	Amino Acid Change
EXT1 (NM_000127.2)		
1	c.138del	p.Leu46Phefs*90
	c.393C>A	p.Tyr131*
	c.679del	p.Arg227Aspfs*25
	c.864del	p.Asn288lysfs*71
2	c.1019G>A	p.Arg340His
	c.1031C>T	p.Ser344Phe
5	c.1384del	p.Leu462Trpfs*11
6	c.1431dup	p.Ser478Leufs*43
7/8	del exon7/exon8	
EXT2 (NM_000249.3)		
2	c.202dup	
6	c.997T>C	p.Val68Glyfs*4
intron 6	c.1039-2A>G	p.Cys333Arg
intron 7	c.1178+1G>A	

EXT indicates exostosin.

After an overnight fast, subjects visited the AMC Vascular Medicine clinical trial unit, where collection of anthropometric data including supine blood pressure measurements and blood collection for plasma biochemistry was performed. Basal fasting glucose, HbA1c, fasting lipid profiles, serum creatinine, and 24-hour urinary albumin excretion were assessed using standard laboratory procedures. Thereafter, flow-mediated dilation (FMD) of the brachial artery was performed as previously described.[7] In short, subjects were in the supine position when a blood pressure cuff was placed just below the elbow of the right arm. The brachial artery in the right antecubital fossa was visualized using a 7.5-MHz transducer. A wall tracking system was used to measure lumen diameter. After the 2 baseline vessel-diameter measurements, reactive hyperemia was induced by inflating the lower-arm blood pressure cuff to 200 mm Hg. Upon release of the cuff after 4 minutes, ultrasonography continued for 5 minutes to allow for lumen diameter measurements at 30-s intervals. Flow-independent vasodilation was assessed after determination of brachial artery diameter before and 4 minutes after the administration of nitroglycerine (0.4 mg). Images were stored digitally and analyzed offline using the Wall Track System software analysis package. One person, who was unaware of clinical details and the stage of the experiment, performed all measurements. At the AMC, intra- and intersession coefficients of variation for baseline diameter assessment using the Wall Track System are 1.1% and 3.8%, respectively. Intersession variability of the FMD measurement is 13.9%.[7]

In Vitro EXT Silencing Experiment in Microvascular Endothelial Cells Under Laminar Flow

Human microvascular endothelial cells (Lonza, Switzerland) were cultured in EGM-2MV medium (Lonza, Switzerland) supplemented with 5% fetal bovine serum (cc-4102B), 0.2 mL corticosone (cc-4112B), 2 mL human fibroblast growth factor (cc-4113B), 0.5 mL vacular endothelial growth factor (cc-4114B), 0.5 mL Rabbit insulin-like growth factor 1 (RB-IGF1) (cc-4115B), 0.5 mL ascorbic acid (cc-4116B), 0.5 mL human endothelial derived factor (hEDF) (cc-4317B), and 0.5 mL Gentamicin and Amphotericin (GA) (cc.4381B) in a humidified incubator at 37°C and 5% CO_2. The flow experiments were performed using an IBIDI Unidirectional Laminar Flow pump system (IBIDI, Martinsried, Germany). IBIDI slides (0.4 mm) were coated with 75 000 cells per slide and incubated for 24 hours in static condition to allow the cells to attach and grow to confluence. The expression of *EXT1* and

Table 2. Human RT-PCR Primer Sequences

Gene	Forward	Reverse
KLF2	5′-cat ctg aag gcg cat ctg-3′	5′- cgt gtg ctt tcg gta gtg g-3′
NRF2	5′-aca cgg tcc aca gct cat c-3′	5′-tgc ctc caa agt atg tca atc a-3′
NOS3	5′-acc ctc acc gct aca aca tc-3′	5′-att tcc act gct gcc ttg tc-3′
EXT1	5′-gct ctt gtc tcg ccc ttt tgt-3′	5′-tgg tgc aag cca ttc cta cc-3′
EXT2	5′- gat tga aga aat gca gag aca gg-3′	5′- tgg ata gat ccg gtc att gat a-3′

EXT indicates exostosin; NOS, nitric oxide synthesis; RT-PCR, reverse-transcription polymerase chain reaction.

EXT2 was suppressed with siRNA (Invitrogen, USA) using 25 nmol/L Dharmafect4 (Thermo Scientific) according to the manufacturer's protocol (n=3 flow experiments per condition). Six hours after transfection of the endothelial cells, the medium was replaced and the flow was started at 30 mL/min (perfusion set selection 15 cm, 1.6 mm; applied pressure:

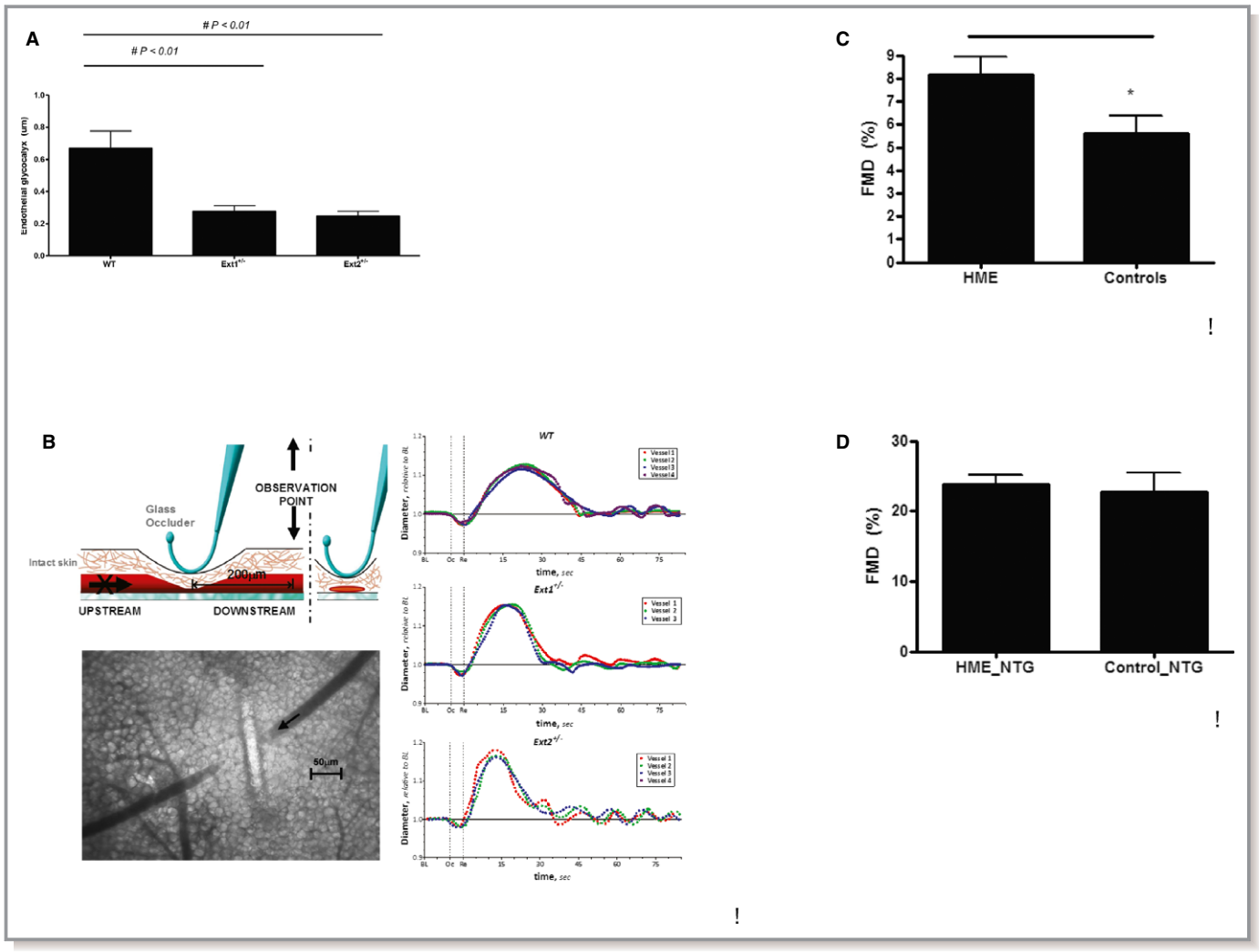

Figure 1. A, In vivo glycocalyx measurements in arterioles in WT mice, *Ext1*$^{+/-}$, and *Ext2*$^{+/-}$ mice (n=7 mice per group). Values are presented as mean±SEM. Differences were analyzed using a nonparametric test (Mann–Whitney). **P*<0.05. B, Graphic overview of single arteriolar vessel occlusion measurement in mice, and example of postdilation FMD curve in WT, *Ext1*$^{+/-}$, and *Ext2*$^{+/-}$ mice as described in detail in the Methods section (n=4 to 6 mice per group analyzed). C, FMD of the brachial artery in controls (n=13) and in HME patients (n=13) with a heterozygous loss of function mutation in *EXT1* or *EXT2*. D, Flow-independent dilation of the brachial artery before and 4 minutes after administration on 0.4 mg nitroglycerine sublingually in controls (n=13) and in HME patients (n=13) with a heterozygous loss of function mutation in *EXT1* or *EXT2.* Values are presented as mean±SEM. Differences were analyzed using a nonparametric test (Mann–Whitney). **P*-value<0.05. EXT indicates exostosin; FMD, flow-mediated dilation; HME, hereditary multiple exostoses; NTG, nitroglycerine; WT, wild-type.

−15 mbar; flow rate: 7.6 mL/min; shear stress: 10 dyne/cm^2, next continuous switching operation 30 s). After 48 hours, the cells were harvested for protein and RNA analysis. The following primers were used to assess the level of suppression by siRNA: *EXT2*: sense 5′-CAG UGU UAG UAC UCG AUA ATT-3′; antisense: UUA UCG AGU ACU AAC ACU Gac-3′; EXT1: sense: 5′GAA GUA UGA UUA UCG GGA Att-3′; antisense: 5′-UUC CCG AUA AUC AUA CUU Ctc-3′. Primers were designed with Primer 3 software and are spanning intron/exon boundaries. As a negative control, we used validated siRNA for GAPDH (Ambion, 4390843).

Cells were directly lysed in TriZol (Invitrogen) for 30 minutes at 4°C. Chloroform was added for phase separation followed by RNA isolation according to the supplier's protocol. RNA samples were then converted to cDNA by reverse transcription reaction (BioRad). Reverse-transcription polymerase chain reaction was performed in a total volume of 10 μL containing Sybr green master mix (GE Biotech), cDNA, and specific primer pairs. Target cDNA was amplified using the CFX 384 system (BioRad) as follows: initial denaturation at 95°C for 10 minutes, followed by 42 cycles of 30 s at 95°C, 1 minute at 55°C for annealing, and 40 s at 72°C for elongation. The amplification was ended with a melting curve starting after 40 cycles. Gene expression was calculated using *RPLP0* (*36B4*) as a housekeeping gene with the ΔΔCt calculation. All experiments were performed at least 4 times. Primer sequences are listed in Table 2.

Table 3. Baseline Characteristics of HME (n=13) and Control Subjects (n=13)

	HME Carriers	Controls	*P* Value
Age, y	40±10	41±10	
Male/female, N	4/9	4/9	
BMI, kg/m^2	23.8±2.9	23.9±2.5	NS
Smoking, N	1	1	
Family history CVD	2	4	
Family history diabetes	3	3	
Cholesterol (C), mmol/L	4.8±0.5	4.5±0.6	0.58
LDL-C, mmol/L	2.5±0.8	2.3±0.4	0.76
HDL-C, mmol/L	1.5±0.3	1.4±0.3	0.53
Triglycerides, mmol/L	0.9 [0.7 to 1.4]	0.8 [0.7 to 1.0]	0.30
Fasting glucose, mmol/L	4.8±0.5	4.9±0.6	0.63
Creatinine, μmol/L	71±11	67±12	0.41
Calculated eGFR, mL/min per 1.73	>60	>60	
CRP, g/L	1.7±1.7	1.2±0.6	0.34
24-h urinary albumin excretion, mg/L	4.8±3.5	4.8±2.5	0.98
SBP, mm Hg	127±11	132±14	0.40
DBP, mm Hg	80±8	78±10	0.70
Mutation in *EXT1/EXT2*	9/4		

Data are presented as mean±SD except for triglycerides, which are presented as median and interquartile range. Data were analyzed using Student *t* test statistics. BMI indicates body mass index; CRP, C-reactive protein; CVD, cardiovascular disease; DBP, diastolic blood pressure; e-GFR, estimated glomerular filtration rate; EXT, exostosin; HDL-C, high-density lipoprotein cholesterol; HME, hereditary multiple exostosis; LDL-C, low-density lipoprotein cholesterol; NS, not significant; SBP, systolic blood pressure.

Western Blotting

In a parallel experiment, endothelial cells were lysed in RIPA buffer with the addition of protease and phosphatase inhibitor cocktails (Roche). Proteins were fractionated on 4% to 12% Bis-Tris sodium dodecyl sulfate polyacrylamide gels and

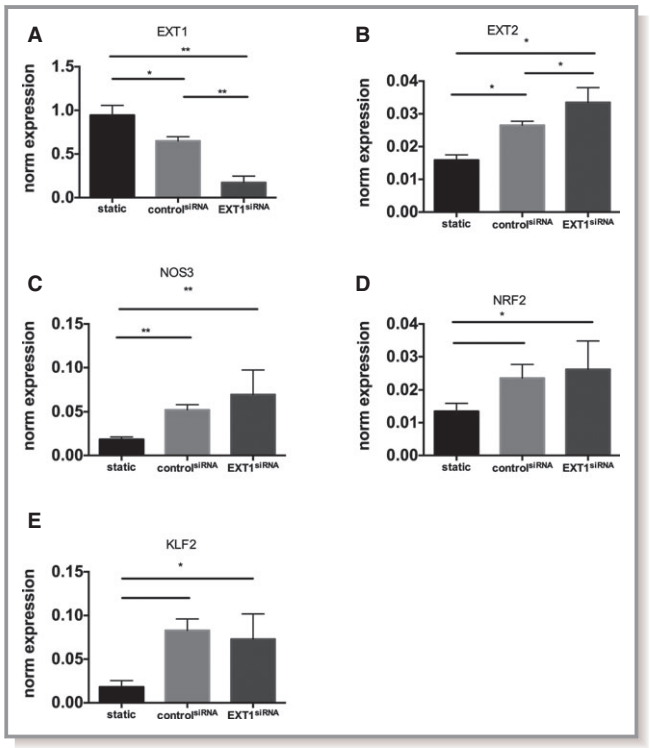

Figure 2. EXT1 knockdown does not lead to further increase in NOS3 pathway. The effect of *EXT1* knockdown on RNA expression of *EXT1* (A), *EXT2* (B), *NOS3* (C), *NRF2* (D), *KLF2* (E) in HMVEC under laminar flow analyzed by RT-PCR. EXT1 was silenced using siRNA against *EXT1* as described. A scrambled siRNA was used as control. Flow induces a significant increase in *NOS3*, nuclear factor erythroid 2–related factor (*NRF2*) and kruppel like factor 2 (*KLF2*), which was not further increased by downregulation of *EXT1*. Data are from 4 independent experiments and presented as mean±SD. All silencing experiments were performed under laminar flow condition. Differences were analyzed using Student *t* test. **P*<0.05; ***P*<0.01. EXT indicates exostosin; HMVEC, human microvascular endothelial cell; KLF2, kruppel like factor 2; NOS, nitric oxide synthesis; NRF-2, nuclear factor erythroid 2–related factor; RT-PCR, reverse-transcription polymerase chain reaction.

transferred to nitrocellulose membranes using the Trans Blot Turbo System (BioRad). The primary antibody dilutions for Western blots were 1:1000 for rabbit anti-human phospho-endothelial nitric oxide synthesis (eNOS) (ser1177, Cell Signalling); 1:1000 for rabbit anti-human eNOS; 1:1000 for rabbit (Cell Signalling), 1:1000 for rabbit anti-human AKT2 (Cell Signalling CST-4691S); and 1:2000 for rabbit anti-human phospho-AKT2 Ser473 (Cell Signalling CST-4060S). The membranes were then incubated with swine anti-rabbit horseradish peroxidase–linked IgG antibody (1:3000; Dako, P0399) or rabbit anti-goat horseradish peroxidase–linked IgG antibody (1:3000; DAKO, P0160) followed by detection of the proteins using femto ECL chemiluminescent horseradish peroxidase substrate (Thermo Scientific) and the ChemiDoc XRS system (BioRad). β-Actin (rabbit anti-human actin; Abcam, ab8227; 1:5000) was used as loading control.

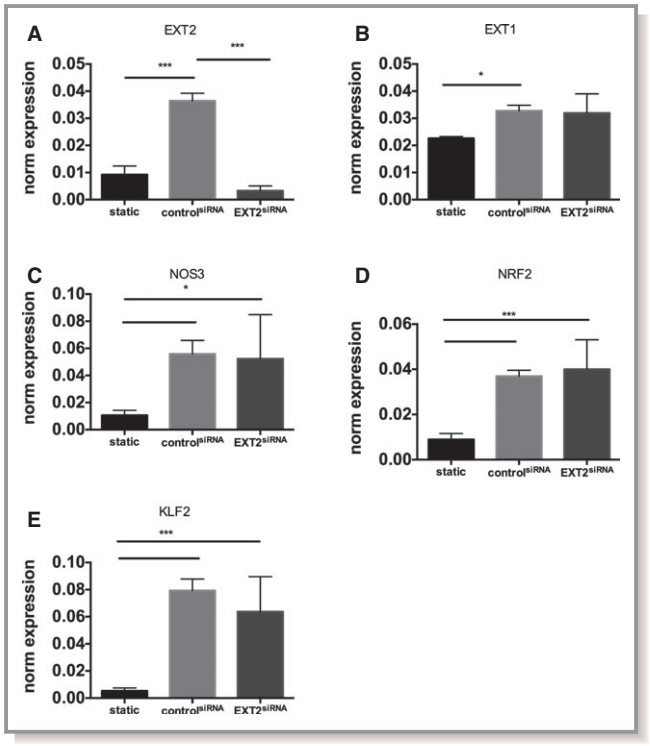

Figure 3. EXT2 knockdown does not lead to further increase in NOS3 pathway. The effect of *EXT2* knockdown on RNA expression of *EXT2* (A), *EXT2* (B), *NOS3* (C), *NRF2* (D), *KLF2* (E) in HMVEC under laminar flow analyzed by RT-PCR. EXT1 was silenced using siRNA against *EXT2* as described. A scrambled siRNA was used as control. Flow induces a significant increase in *NOS3*, *NRF2,* and *KLF2*, which was not further increased by downregulation of *EXT2*. Data are from 4 independent experiments and presented as mean±SD. All silencing experiments were performed under laminar flow condition. Differences were analyzed using a nonparametric statistical test (Mann–Whitney). Differences were analyzed using Student *t* test. **P*<0.05; ****P*<0.005. EXT indicates exostosin; HMVEC, human microvascular endothelial cell; KLF2, kruppel like factor 2; NOS, nitric oxide synthesis; NRF-2, nuclear factor erythroid 2–related factor; RT-PCR, reverse-transcription polymerase chain reaction.

Statistical Analysis

The data are presented as means±SD or where indicated mean±SEM. Differences between *EXT* heterozygotes and controls were calculated by nonparametric tests (Mann–Whitney) or by *t* test statistics depending on the distribution of the data. The effect of $EXT1^{SiRNA}$ and $EXT2^{siRNA}$ treatment were compared with $control^{siRNA}$ by nonparametric Kruskal–Wallis statistics. $P<0.05$ was considered significant. Statistical analyses were performed using SPSS package version 20.

Results

Dimensional and Functional Endothelial Changes in Genetically Modified Ext1 and Ext2 Mice

We examined hemodynamic features in genetically modified *Ext1* and *Ext2* mice. Endothelial glycocalyx dimensions in arterioles were significantly altered in both $Ext1^{+/-}$ and $Ext2^{+/-}$ mouse as compared to WT mice (WT: 0.67±0.1 μm, $Ext1^{+/-}$: 0.28±0.1 μm and $Ext2^{+/-}$: 0.25±0.1 μm, $P<0.01$; n=7 mice per group; Figure 1A). Vessel diameter tended to decrease slightly upon short-term single arteriolar vessel occlusion in all animals due to reduction of intravascular pressure (data not shown), with FMD taking place in all groups after reperfusion. Selected examples of FMD for WT, $Ext1^{+/-}$ and $Ext2^{+/-}$ mice are presented in Figure 1B. Maximal arteriolar dilation during reperfusion was significantly greater for both $Ext1^{+/-}$ (15.2±1.4% vasodilation; 12 arterioles with diameter of 51±6 μm; n=4 mice, $P<0.05$) and $Ext2^{+/-}$ (13.8±1.6% vasodilation, 10 arterioles with diameter of 49±8 μm; n=4 mice, $P<0.05$) compared to WT (11.3±1.0% vasodilation, 20 arterioles with diameter of 53±4 μm; n=6 mice). The time at which the maximal dilation was reached occurred more quickly after reperfusion in $Ext1^{+/-}$ (17.4±2.0 s, $P<0.05$) and $Ext2^{+/-}$ (15.8±1.7 s, $P<0.05$) mice compared to the WT mice (23.2±2.3 s). FMD values were also calculated as the square of the diameter change, times the dilation time. These calculated FMD values also showed a significant increase in $Ext1^{+/-}$ (4.5±0.5 s, $P<0.05$) and $Ext2^{+/-}$ (3.9±0.4 s, $P<0.01$) mice compared to the WT mice (3.3±0.3 s).

Dimensional and Functional Endothelial Changes in Humans Carrying Heterozygous Loss of Function Mutations in EXT

Next, we investigated whether the presence of heterozygous loss of function mutations in *EXT* in human subjects leads to aberrant endothelial function compared to normal control

subjects. Age, body mass index, family history of diabetes and cardiovascular disease, as well as plasma biochemistry and 24-hour urinary albumin excretion were comparable between 13 HME carriers and 13 control subjects (Table 3). A significant increase in FMD was observed between *EXT* mutation carriers as compared to age- and sex-matched controls (*EXT*: 8.1±0.8% versus controls 5.6±0.7%, $P<0.05$). When patients were challenged with a NO-donor (sublingual nitroglycerin) as a measurement of endothelium-independent vasodilatation, vasodilation was induced to the same extent in carriers and controls (EXT: 23.7±1.4% versus 22.8±2.6%, ns; Figure 1C and 1D).

Effect of EXT-Silencing on Gene Expression in Human Microvascular Endothelial Cells Under Flow Conditions

To gain more insight into the mechanism explaining observed changes in *EXT* loss of function mutants, we silenced *EXT1* or *EXT2* expression in human microvascular endothelial cells cultured under laminar flow. Exposure to flow induced a significant increase in *EXT2* ($P<0.005$) but a small but significant reduction in *EXT1* expression ($P<0.05$) (Figures 2 and 3). Flow exposure also significantly induced *NOS3, NRF2,* and *KLF2* expression (n=3 experiments, $P<0.05$). Silencing of *EXT1* and *EXT2* was effective, resulting in a decreased expression of 60% to 80% of the targeted gene (Figures 2A and 3A). Under these conditions, however, no further increase in flow-induced expression of *NOS3*, *NRF2,* and *KLF2* was found (n=3 experiments, Figures 2B through D and 3B through D). We subsequently tested whether silencing of *EXT1* or *EXT2* results in a change in eNOS protein expression and eNOS phosphorylation. Induction of flow resulted in a significantly increased eNOS protein ($P<0.05$) and phosphorylation of eNOS ($P<0.05$) (n=3 experiments, Figures 4 and 5) but the ratio of phospho-eNOS/eNOS was not significantly different. Silencing of *EXT1* or *EXT2* resulted in an increased eNOS protein expression in both conditions ($P<0.05$), and phosphorylation status ($P<0.05$) as compared to (scrambled)

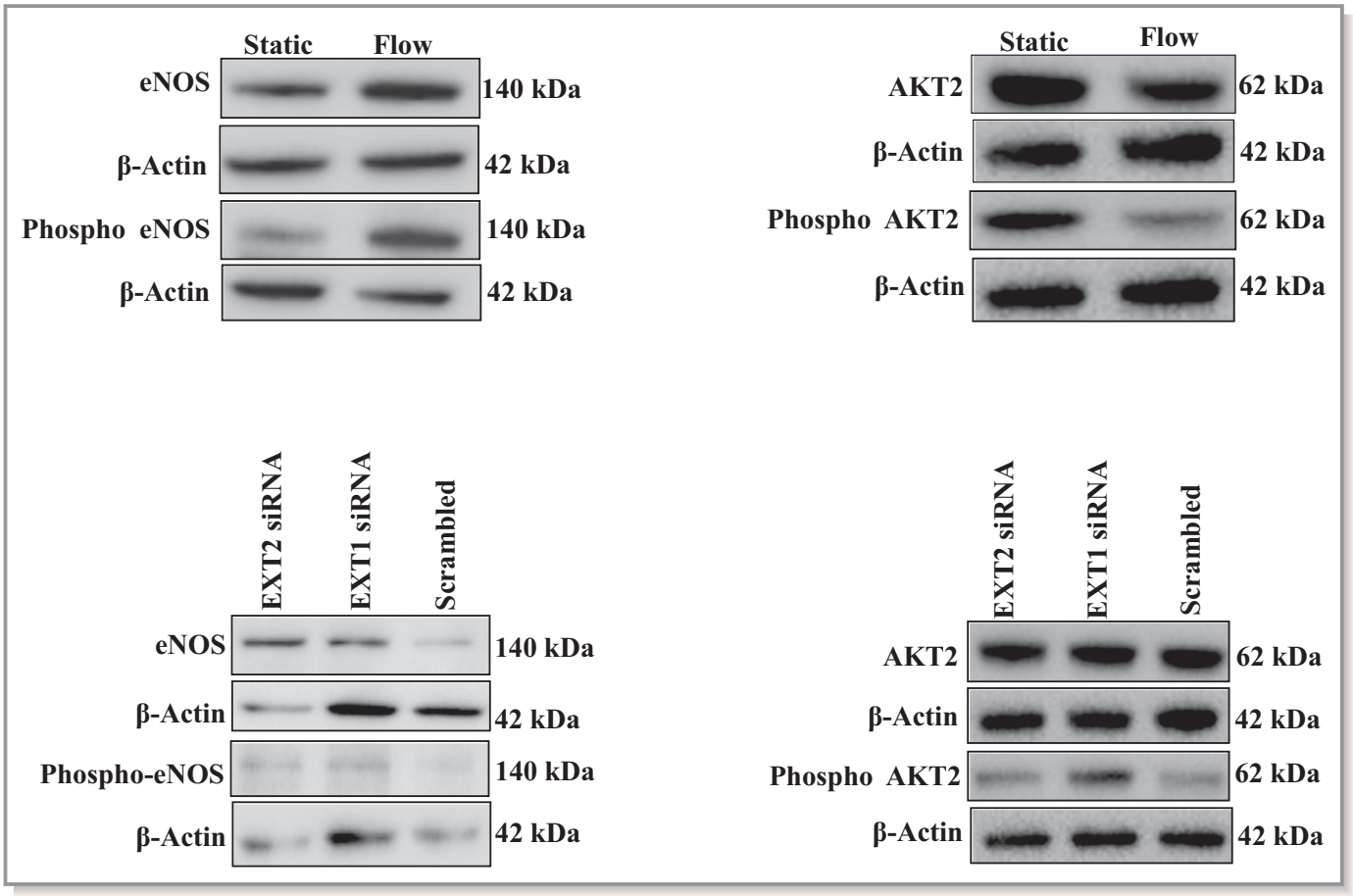

Figure 4. Protein expression of eNOS, phospho-eNOS, AKT and phospho-AKT2 in HMVEC under static and laminar flow conditions. An example of eNOS, p-eNOS, (left panel) AKT2 and p-AKT2 protein expression (right panel) in HMVEC cell lysates under static and flow conditions with or without $EXT1^{siRNA}$ or $EXT2^{siRNA}$. HMVECs were transfected with $EXT1^{siRNA}$ or $EXT2^{siRNA}$, after which cells were studied under laminar flow. β-Actin was used as loading control. eNOS indicates endothelial nitric oxide synthesis; EXT, exostosin; HMVEC, human microvascular endothelial cell.

control. The ratio phospho-eNOS/eNOS was significantly reduced under the EXT2^{siRNA} treatment but not under EXT1^{siRNA} condition (Figure 5B through 5D). Additionally, we measured the capacity of these human microvascular endothelial cells to phosphorylate AKT2, which may explain the underlying mechanism of increased eNOS expression. Induction of flow resulted in a significant decrease in AKT2 and phospho-AKT2 (n=3 experiments), yet the ratio remained unchanged (Figure 5B through 5F). In line, silencing of EXT1 and EXT2 did not show significant differences in AKT2 protein and phosphorylation status (Figure 5E through 5H).

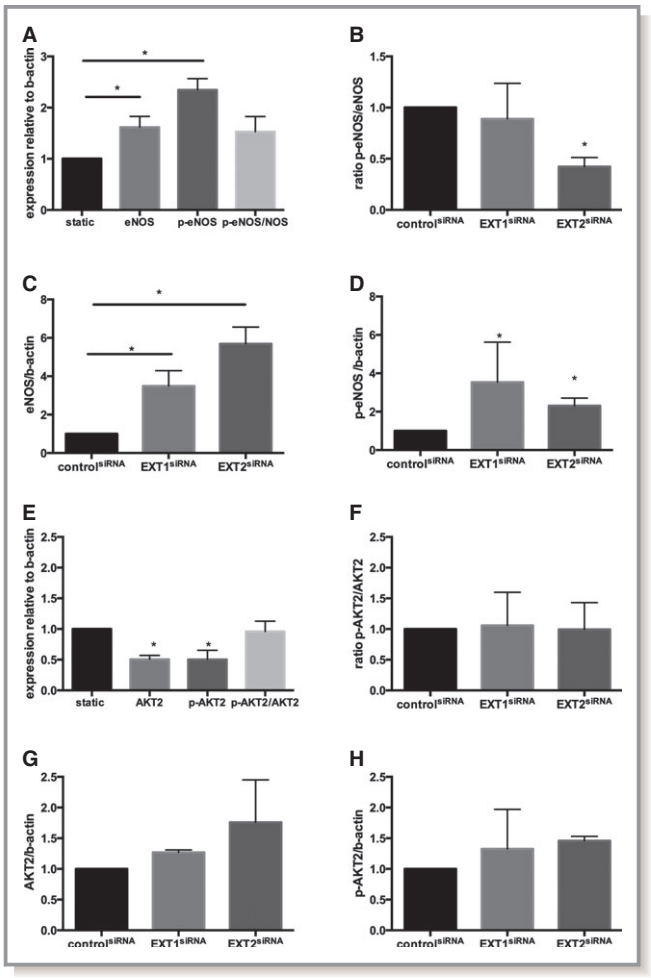

Figure 5. Protein expression of eNOS, phospho-eNOS, AKT, and phospho-AKT2 in HMVEC under static and laminar flow conditions. A, The protein expression of eNOS, p-eNOS, and the ratio of p-eNOS/eNOS under flow as well as static condition. B, Effect of *EXT1*^{siRNA} or *EXT2*^{siRNA} on eNOS protein expression. C, Effect of *EXT1*^{siRNA} or *EXT2*^{siRNA} on phospho-eNOS protein expression. D, Effect of *EXT1*^{siRNA} or *EXT2*^{siRNA} on the ratio of phospho-eNOS/eNOS protein expression. All data are presented as mean±SEM (n=3 experiments). Differences between control and treatment groups were analyzed using nonparametric Kruskal–Wallis statistics. *P<0.05. E, Effect of flow on induction of AKT2 protein expression and phosphorylation status. F, Effect of *EXT1*^{siRNA} or *EXT2*^{siRNA} on AKT2 protein expression. G, Effect of *EXT1*^{siRNA} or *EXT2*^{siRNA} on phospho-AKT2 protein expression. H, Effect of *EXT1*^{siRNA} or *EXT2*^{siRNA} on the ratio of phospho-AKT2/AKT2 protein expression. Data are presented as mean±SEM for n=3 experiments. Differences between control and treatment groups were analyzed using nonparametric Kruskal–Wallis statistics. *P<0.05. eNOS indicates endothelial nitric oxide synthesis; EXT, exostosin; HMVEC, human microvascular endothelial cell.

Discussion

In the present study, we show that heterozygous loss of function of *EXT1* and *EXT2,* both in humans as well as mice, results in a decreased arteriolar endothelial glycocalyx but improved FMD. Moreover, silencing of *EXT1* or *EXT2* in human microvascular endothelial cells cultured under laminar flow conditions revealed a similar change in endothelial NO metabolism, predominantly due to the increased NO synthase protein and phosphorylation of NO synthase, whereas AKT2 protein and phosphorylation status was unchanged. Our findings imply that genetic mutations in endothelial HSPG chain length adversely affect endothelial glycocalyx dimension but lead to increased NO availability.[27] Together these data suggest that endothelial HSPGs are involved in cardiovascular homeostasis.

Differential Effects of Enzymatic Versus Genetic HSPG Alterations in Endothelial Glycocalyx

The endothelial glycocalyx consists of a glycosaminoglycan layer covering the endothelium and constitutes a conductive, gel-like layer between the flowing blood and the endothelial cells in both the micro- and macrocirculation.[28] Shear stress exerted to the endothelium by flowing blood has been widely recognized as the principal stimulus for continuous endothelial NO release,[28] providing a first-line defense against adhering platelets and subsequent atherothrombosis.[10] Complete removal of this glycosaminoglycan layer, using either exogenous hyaluronidase or heparinases, has been shown to disrupt this mechanotransductor function leading to impaired shear-mediated NO release[5,6,28,29] and accelerated atherosclerosis in mice.[11,27] Current evidence of endothelial glycocalyx composition on endothelial barrier function is based on studies applying exogenous enzymatic removal in vitro[30] and in vivo, showing that removal of endothelial HSPG chains by heparanase was associated with the presence of microalbuminuria.[29,31] In contrast, kidney conditional *Ndst1* knockout mice did not show any signs of microalbuminuria, underscoring the potential difference in pathophysiological effect on endothelial function of acquired (exogenous enzyme) and inborn (genetic) HSPG defects.[32]

Altered HSPG in Relation to NO-Bioavailability in EXT Mutants

HSPG synthesis and sulfation is driven by >20 different genes, of which the enzymes EXT and EXTL are involved in heparan sulfate chain elongation.[14,33,34] Moreover, it was shown that a knockdown of either *EXT1* or *EXT2* affects expression and function of other HSPG synthesizing genes, which subsequently can influence heparan sulfate structure and functionality.[35] Of note, as combined homozygote mutations of both *EXT1* and *EXT2* are not compatible with life in HME patients,[14,18] we have not performed these siRNA experiments in human microvascular endothelial cells due to lack of clinical relevance. In conclusion, our data imply that decreased glycocalyx dimension in heterozygous *EXT* mutants is associated with improved mechanotransduction of shear stress into activation of endothelial NO-release;[36] however, this does not seem to be mediated via AKT2.[9] Shear-stress-induced NO release is mediated by 2 pathways: increased calcium influx mediating NOS-activation in a calmodulin-dependent manner,[37] and increased phosphorylation of eNOS.[38] In this respect, it is interesting to note that HSPGs (eg, glypican-1) cluster with caveolin in endothelial lipid rafts upon exposure to shear stress.[39]

In conclusion, our findings underscore the complex interaction between exposed shear stress of the endothelium, endothelial glycocalyx HSPG composition, and subsequent endothelial NO-release. Since our data imply that endothelial EXT1 and EXT2 are involved in NO bioavailability, endothelial heparan sulfates might be interesting therapeutic targets for endothelial dysfunction and subsequent cardiovascular disease in humans.

Author Contributions

Nieuwdorp, Intaglietta, Esko, Kastelein, and Stroes designed the study. Mooij, Cabrales, Bernelot Moens, Xu, Tsai, Sande, Dallinga-Thie, and Nieuwdorp performed the research. Groot provided analytic tools. Mooij, Cabrales, Esko, Stroes, and Nieuwdorp drafted the paper; all authors critically reviewed the manuscript.

Acknowledgments

We are grateful to all participating HME subjects and Jan de Lange from the Dutch HME Foundation (www.hme-mo.nl) for their help with inclusion and being able to perform this study. We thank J.A. Sierts for assistance with the in vitro studies.

Sources of Funding

We acknowledge the support from the Netherlands Cardio-Vascular Research Initiative: the Dutch Heart Foundation, Dutch Federation of University Medical Centres, the Netherlands Organisation for Health Research and Development, and the Royal Netherlands Academy of Scíences. Nieuwdorp: NWO-VENI grant 2008 (016.096.044), Esko (NIH Program Projects HL107150 and HL057345), Bernelot Moens and Stroes: grant from CVON (GENIUS) (number CVON2011-19), Kastelein is a recipient of the Lifetime Achievement Award of the Netherlands Heart Foundation (NHS, project number 2010T082). Dr Intaglietta: R24-HL064395 and R01-HL06 2354; Dr Cabrales: R01-HL52684 and Dr Tsai: W81XWH 1120012.

Disclosures

None.

References

1. Murray CJ, Richards MA, Newton JN, Fenton KA, Anderson HR, Atkinson C, Bennett D, Bernabe E, Blencowe H, Bourne R, Braithwaite T, Brayne C, Bruce NG, Brugha TS, Burney P, Dherani M, Dolk H, Edmond K, Ezzati M, Flaxman AD, Fleming TD, Freedman G, Gunnell D, Hay RJ, Hutchings SJ, Ohno SL, Lozano R, Lyons RA, Marcenes W, Naghavi M, Newton CR, Pearce N, Pope D, Rushton L, Salomon JA, Shibuya K, Vos T, Wang H, Williams HC, Woolf AD, Lopez AD, Davis A. UK health performance: findings of the Global Burden of Disease Study 2010. *Lancet*. 2013;381:997–1020.
2. Rudolph V, Freeman BA. Cardiovascular consequences when nitric oxide and lipid signaling converge. *Circ Res*. 2009;105:511–522.
3. Flammer AJ, Anderson T, Celermajer DS, Creager MA, Deanfield J, Ganz P, Hamburg NM, Luscher TF, Shechter M, Taddei S, Vita JA, Lerman A. The assessment of endothelial function: from research into clinical practice. *Circulation*. 2012;126:753–767.
4. Tarbell JM, Ebong EE. The endothelial glycocalyx: a mechano-sensor and -transducer. *Sci Signal*. 2008;1:pt8.
5. Mochizuki S, Vink H, Hiramatsu O, Kajita T, Shigeto F, Spaan JA, Kajiya F. Role of hyaluronic acid glycosaminoglycans in shear-induced endothelium-derived nitric oxide release. *Am J Physiol Heart Circ Physiol*. 2003;285:H722–H726.
6. Florian JA, Kosky JR, Ainslie K, Pang Z, Dull RO, Tarbell JM. Heparan sulfate proteoglycan is a mechanosensor on endothelial cells. *Circ Res*. 2003;93:e136–e142.
7. Nieuwdorp M, van Haeften TW, Gouverneur MC, Mooij HL, van Lieshout MH, Levi M, Meijers JC, Holleman F, Hoekstra JB, Vink H, Kastelein JJ, Stroes ES. Loss of endothelial glycocalyx during acute hyperglycemia coincides with endothelial dysfunction and coagulation activation in vivo. *Diabetes*. 2006;55:480–486.
8. Nieuwdorp M, Meuwese MC, Mooij HL, Ince C, Broekhuizen LN, Kastelein JJ, Stroes ES, Vink H. Measuring endothelial glycocalyx dimensions in humans: a potential novel tool to monitor vascular vulnerability. *J Appl Physiol (1985)*. 2008;104:845–852.
9. Koo A, Dewey CF Jr, Garcia-Cardena G. Hemodynamic shear stress characteristic of atherosclerosis-resistant regions promotes glycocalyx formation in cultured endothelial cells. *Am J Physiol Cell Physiol*. 2013;304:C137–C146.
10. Meuwese MC, Broekhuizen LN, Kuikhoven M, Heeneman S, Lutgens E, Gijbels MJ, Nieuwdorp M, Peutz CJ, Stroes ES, Vink H, van den Berg BM. Endothelial surface layer degradation by chronic hyaluronidase infusion induces proteinuria in apolipoprotein E-deficient mice. *PLoS One*. 2010;5:e14262.
11. Planer D, Metzger S, Zcharia E, Wexler ID, Vlodavsky I, Chajek-Shaul T. Role of heparanase on hepatic uptake of intestinal derived lipoprotein and fatty streak formation in mice. *PLoS One*. 2011;6:e18370.
12. Nikmanesh M, Shi ZD, Tarbell JM. Heparan sulfate proteoglycan mediates shear stress-induced endothelial gene expression in mouse embryonic stem cell-derived endothelial cells. *Biotechnol Bioeng*. 2012;109:583–594.
13. Zeng Y, Ebong EE, Fu BM, Tarbell JM. The structural stability of the endothelial glycocalyx after enzymatic removal of glycosaminoglycans. *PLoS One*. 2012;7:e43168.
14. Forsberg E, Kjellen L. Heparan sulfate: lessons from knockout mice. *J Clin Invest*. 2001;108:175–180.

15. Lind T, Tufaro F, McCormick C, Lindahl U, Lidholt K. The putative tumor suppressors EXT1 and EXT2 are glycosyltransferases required for the biosynthesis of heparan sulfate. *J Biol Chem*. 1998;273:26265–26268.
16. Bishop JR, Schuksz M, Esko JD. Heparan sulphate proteoglycans fine-tune mammalian physiology. *Nature*. 2007;446:1030–1037.
17. Duncan G, McCormick C, Tufaro F. The link between heparan sulfate and hereditary bone disease: finding a function for the EXT family of putative tumor suppressor proteins. *J Clin Invest*. 2001;108:511–516.
18. Zak BM, Schuksz M, Koyama E, Mundy C, Wells DE, Yamaguchi Y, Pacifici M, Esko JD. Compound heterozygous loss of EXT1 and EXT2 is sufficient for formation of multiple exostoses in mouse ribs and long bones. *Bone*. 2011;48:979–987.
19. Wuyts W, Van Hul W, De Boulle K, Hendrickx J, Bakker E, Vanhoenacker F, Mollica F, Ludecke HJ, Sayli BS, Pazzaglia UE, Mortier G, Hamel B, Conrad EU, Matsushita M, Raskind WH, Willems PJ. Mutations in the EXT1 and EXT2 genes in hereditary multiple exostoses. *Am J Hum Genet*. 1998;62:346–354.
20. Schmale GA, Conrad EU III, Raskind WH. The natural history of hereditary multiple exostoses. *J Bone Joint Surg Am*. 1994;76:986–992.
21. Hecht JT, Hall CR, Snuggs M, Hayes E, Haynes R, Cole WG. Heparan sulfate abnormalities in exostosis growth plates. *Bone*. 2002;31:199–204.
22. Anower EKMF, Matsumoto K, Habuchi H, Morita H, Yokochi T, Shimizu K, Kimata K. Glycosaminoglycans in the blood of hereditary multiple exostoses patients: half reduction of heparan sulfate to chondroitin sulfate ratio and the possible diagnostic application. *Glycobiology*. 2013;23:865–876.
23. Cabrales P, Tsai AG, Frangos JA, Intaglietta M. Role of endothelial nitric oxide in microvascular oxygen delivery and consumption. *Free Radic Biol Med*. 2005;39:1229–1237.
24. Vink H, Duling BR. Identification of distinct luminal domains for macromolecules, erythrocytes, and leukocytes within mammalian capillaries. *Circ Res*. 1996;79:581–589.
25. Intaglietta M, Tompkins WR. Microvascular measurements by video image shearing and splitting. *Microvasc Res*. 1973;5:309–312.
26. Goud AL, de Lange J, Scholtes VA, Bulstra SK, Ham SJ. Pain, physical and social functioning, and quality of life in individuals with multiple hereditary exostoses in the Netherlands: a National Cohort Study. *J Bone Joint Surg*. 2012;94:1013–1020.
27. Baker AB, Groothuis A, Jonas M, Ettenson DS, Shazly T, Zcharia E, Vlodavsky I, Seifert P, Edelman ER. Heparanase alters arterial structure, mechanics, and repair following endovascular stenting in mice. *Circ Res*. 2009;104:380–387.
28. Broekhuizen LN, Mooij HL, Kastelein JJ, Stroes ES, Vink H, Nieuwdorp M. Endothelial glycocalyx as potential diagnostic and therapeutic target in cardiovascular disease. *Curr Opin Lipidol*. 2009;20:57–62.
29. Gil N, Goldberg R, Neuman T, Garsen M, Zcharia E, Rubinstein AM, van Kuppevelt T, Meirovitz A, Pisano C, Li JP, van der Vlag J, Vlodavsky I, Elkin M. Heparanase is essential for the development of diabetic nephropathy in mice. *Diabetes*. 2012;61:208–216.
30. Cho HJ, Xie QW, Calaycay J, Mumford RA, Swiderek KM, Lee TD, Nathan C. Calmodulin is a subunit of nitric oxide synthase from macrophages. *J Exp Med*. 1992;176:599–604.
31. Deckert T, Feldt-Rasmussen B, Borch-Johnsen K, Jensen T, Kofoed-Enevoldsen A. Albuminuria reflects widespread vascular damage. The steno hypothesis. *Diabetologia*. 1989;32:219–226.
32. Sugar T, Wassenhove-McCarthy DJ, Esko JD, van Kuppevelt TH, Holzman L, McCarthy KJ. Podocyte-specific deletion of NDST1, a key enzyme in the sulfation of heparan sulfate glycosaminoglycans, leads to abnormalities in podocyte organization in vivo. *Kidney Int*. 2014;85:307–318.
33. Esko JD, Lindahl U. Molecular diversity of heparan sulfate. *J Clin Invest*. 2001;108:169–173.
34. Busse M, Feta A, Presto J, Wilen M, Gronning M, Kjellen L, Kusche-Gullberg M. Contribution of EXT1, EXT2, and EXTL3 to heparan sulfate chain elongation. *J Biol Chem*. 2007;282:32802–32810.
35. Presto J, Thuveson M, Carlsson P, Busse M, Wilen M, Eriksson I, Kusche-Gullberg M, Kjellen L. Heparan sulfate biosynthesis enzymes EXT1 and EXT2 affect NDST1 expression and heparan sulfate sulfation. *Proc Natl Acad Sci USA*. 2008;105:4751–4756.
36. Kang H, Fan Y, Deng X. Vascular smooth muscle cell glycocalyx modulates shear-induced proliferation, migration, and no production responses. *Am J Physiol Heart Circ Physiol*. 2011;300:H76–H83.
37. Mittal CK, Jadhav AL. Calcium-dependent inhibition of constitutive nitric oxide synthase. *Biochem Biophys Res Commun*. 1994;203:8–15.
38. Figueroa XF, Gonzalez DR, Puebla M, Acevedo JP, Rojas-Libano D, Duran WN, Boric MP. Coordinated endothelial nitric oxide synthase activation by translocation and phosphorylation determines flow-induced nitric oxide production in resistance vessels. *J Vasc Res*. 2013;50:498–511.
39. Zeng Y, Waters M, Andrews A, Honarmandi P, Ebong EE, Rizzo V, Tarbell JM. Fluid shear stress induces the clustering of heparan sulfate via mobility of glypican-1 in lipid rafts. *Am J Physiol Heart Circ Physiol*. 2013;305:H811–H820.